Compressive Failure of Sandwich Beams with Debonded Face-Sheets

JOHN L. AVERY III[1] AND BHAVANI V. SANKAR[2]
Department of Aerospace Engineering
Mechanics & Engineering Science
P.O. Box 116250
University of Florida
Gainesville, FL 32611-6250

(Received December 20, 1998)
(Revised May 20, 1999)

ABSTRACT: Axial compression tests were performed on debonded sandwich composites made of graphite/epoxy face-sheets and aramid fiber honeycomb core. The sandwich beams were manufactured using a vacuum bagging process. The face-sheet and the sandwich beam were cocured. Delamination between one of the face-sheets and the core was introduced by using a Teflon® layer during the curing process. Axial compression tests were performed to determine the ultimate load carrying capacity of the debonded beams. Flatwise tension tests and Double Cantilever Beam tests were performed to determine, respectively, the strength and fracture toughness of the face-sheet/core interface. From the test results semi-empirical formulas were derived for the fracture toughness and ultimate compressive load carrying capacity in terms of the core density, core thickness, face-sheet thickness and debond length. Four different failure modes and their relation to the structural properties were identified. Linear buckling analysis was found to be inadequate in predicting the compressive load carrying capacity of the debonded sandwich composites.

KEY WORDS: buckling, compressive strength, debonding, delamination, fracture toughness, honeycomb core, post-buckling, sandwich beams, sandwich construction.

1. INTRODUCTION

THERE IS A renewed interest in using sandwich construction in aerospace structures mainly driven by the possibility of reducing weight and cost. Fiber composites such as graphite/epoxy are favored as the face-sheet material because of their high stiffness and ability to be co-cured with many core materials. In aeronautical applications sandwich constructions find applications in wing skins and

[1]Currently with Scaled Composites, Mojave, CA.
[2]Author to whom correspondence should be addressed.

0021-9983/00/14 1176–24 $10.00/0

fuselage among other structures. Debonding of the face-sheet from the core is a serious problem in sandwich constructions. This may occur during the fabrication process due to inadvertent introduction of foreign matter at the interface or due to severe loads as in foreign object impact. The debonded sandwich panels are susceptible to buckling under in-plane compressive loads, which may lead to the propagation of the delamination, and/or core and face-sheet failure. Hence there is a need for a systematic study to understand how the core and face-sheet properties affect the compression behavior of a debonded sandwich composite.

There are many works concerning buckling of delaminated composite beams and plates. These models were later extended to sandwich beams. Simitses et al. (1985) and Yin et al. (1986) developed analytical models to study the effects of delamination on the ultimate load capacity of beam plates. The latter paper included the post-buckling behavior as well as energy release rate calculations to predict delamination growth. Chen (1993) included the transverse shear effects on buckling, post-buckling and delamination growth in one-dimensional plates. A nonlinear solution method was developed by Kassapoglou (1988) for buckling and post-buckling of elliptical delaminations under compressive loads. This method employs a series solution method in conjunction with the perturbation technique to solve the laminated plate equations for large deflection. Experiments were performed on sandwich panels containing delaminated face-sheets (note that the delaminations were in between layers of the face-sheet; the face-sheet/core interface did not contain delaminations). The nonlinear models were able to predict the onset of delamination and failure loads in the experiments.

Minguet et al. (1987) studied the compressive failure of sandwich panels with a variety of core materials including honeycomb core. They observed three types of failure modes—core failure, disbond and face-sheet fracture. Based on the test results they developed a nonlinear model to predict these failures using appropriate failure criterion for each failure mode. Sleight and Wang (1995) compared various approximate numerical techniques for predicting the buckling loads of debonded sandwich panels, and compared them with plane finite element analysis. They concluded that 2-D plane strain FE analysis is necessary in order to predict the buckling loads accurately. Hwu and Hu (1992) extended the work of Yin et al. (1986) for the case of debonded sandwich beams. They developed formulas for buckling loads in terms of sandwich beam properties and debond length. Kim and Dharan (1992) used a beam on elastic foundation model and computed the energy release rate in debonded sandwich panels. Based on fracture mechanics they predicted critical debond lengths for crack propagation. They used their model to predict failure in plastic-foam core sandwich panels. An extensive experimental study was conducted by Kardomateas (1990) to understand the buckling and post-buckling behavior of delaminated Kevlar®/epoxy laminates. The experimental program documented the load-deflection diagrams, deformation shape in post-buckling and growth of delamination.

From this literature survey it is clear that a systematic study of compression behavior of sandwich panels with debonded face-sheets, especially failure in the post-buckling regime, is overdue. Any modeling should be preceded by a testing program to understand the effects of various parameters such as face-sheet stiffness, core stiffness and core thickness, and debond length on the buckling and post-buckling behavior. In the present study an experimental program has been undertaken to achieve the aforementioned objectives.

2. MATERIALS AND METHODS

2.1 Material System

The sandwich composites used in this study consisted of graphite/epoxy face-sheets and aramid honeycomb core. The face-sheet was a laminated plain-woven composite fabricated using prepregs manufactured by Fibrite (product number HMF 5-322D/97714AC). Some properties provided by the manufacturer (55%–60% fiber volume) are given in Table 1. The core material used is an aramid honeycomb manufactured by Euro-Composites. It is made up of an aramid fabric bonded together and expanded to form little hexagonal cells. This structure is then coated with a phenolic resin. The honeycomb structure has orthotropic properties, and its principal material directions are denoted by L, W, and t. As depicted in Figure 1 the L-direction, the ribbon direction, refers to the direction in which the constituent tapes lie and are bonded together. The W-direction is in the plane of the material, but perpendicular to the L-direction. The t-direction is through-the-thickness direction.

An optional addition to the sandwich composite is an adhesive film. Generally, this layer is added between the face-sheet and the core to ensure a good interface bond, but at the cost of increase in the weight and cost of the structure.

In the present study the face-sheet consisted of 1, 3, 5 or 7 plies of the graphite/epoxy cloth. All the plies were oriented at 0° direction with respect to the L-direction of the core. The nominal thickness of the face-sheet after curing was 0.22×10^{-3} m (8.7×10^{-3} in.) per ply. Three different core materials with densities 29, 48

Table 1. Properties of the graphite/epoxy face-sheet material.

Compressive strength	531 MPa (77 ksi)
Tensile strength	669 MPa (97 ksi)
Tensile modulus	53 GPa (7.7 msi)
Tensile strain (max.)	12,658 $\mu\epsilon$
Flatwise tensile strength	4.78 MPa (693 psi)
Pre-cured resin content	41.0% by volume

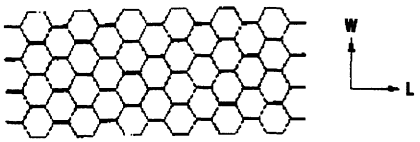

Figure 1. *Principal directions of the honeycomb core.*

and 96 kg/m^3 [1.8, 3 and 6 pcf (pounds per cubic feet)] were used. Further, these core materials were available in three thicknesses: 6.35×10^{-3} m, 9.525×10^{-3} m, and 12.7×10^{-3} m (0.25, 0.375 and 0.5 inches). Thus, there were 9 different core configurations available for testing. The cell size for all core materials was 3.2×10^{-3} m (0.125 in.). The transverse shear properties of the core are available from the manufacturer, and are presented in Table 2. Some standard tests were performed to measure in-plane properties (Avery, 1998). For the 6 pcf core the Young's moduli in the *L*- and *W*-directions, respectively, were 7.73 MPa (1,121 psi) and 4.17 MPa (604 psi). The tensile strength in the *W*-direction is controlled by the bonding between the tapes, and is measured to be about 0.21 MPa (30.4 psi). The strength in the *L*-direction could not be measured as the core collapses in the *W*-direction during the test, and the strength approaches that of the ribbons used in the manufacture of the core.

2.2 Fabrication Process

The fabrication process used was similar to that used in the production of low cost aircraft components. Also, for speediness and cost reduction, the panels were co-cured, i.e., the face-sheets and the core are bonded while the face-sheet is being cured. The majority of the panels manufactured for these experiments used only the excess epoxy from the face-sheet prepregs to bond to the core material, although the addition of an epoxy film adhesive (Hysol XEA 9695) was tried in some through-the-thickness tensile tests. Delaminations were introduced into the specimen by inserting non-porous Teflon® strips between the prepreg and the honeycomb core. The temperature cycle used for curing is shown in Figure 2. Details

Table 2. Properties of the honeycomb core material.

Core Density kg/m^3 (pcf)	Shear Modulus G_{Lt}, MPa (ksi)	Shear Strength S_{Lt}, MPa (psi)	Shear Modulus G_{Wt}, MPa (ksi)	Shear Strength S_{Wt}, MPa (psi)
29 (1.8)	27 (3.9)	0.62 (90)	16 (2.3)	0.38 (55)
48 (3.0)	48 (7.0)	1.32 (191)	30 (4.4)	0.72 (104)
96 (6.0)	96 (13.9)	2.80 (406)	68 (9.9)	1.68 (244)

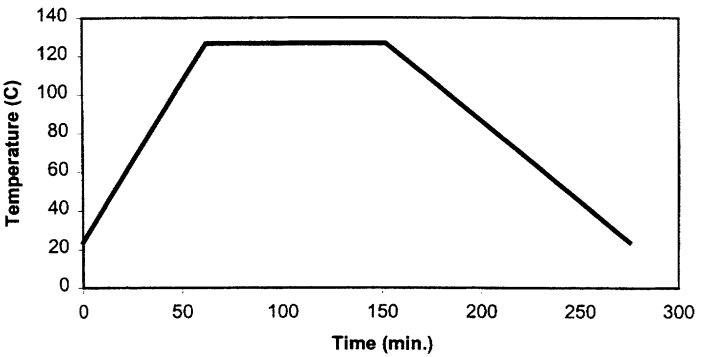

Figure 2. *Temperature cycle used for curing the sandwich composites.*

of the curing procedure including the equipment used can be found in Avery (1998).

2.3 DCB Tests

Double Cantilever Beam Tests (see Figure 3) were performed to estimate the interfacial fracture toughness of the face-sheet/core interface. Specimens were manufactured from a flat sandwich plate containing a 1-inch non-porous Teflon strip between the face-sheet and core material. This Teflon® sheet induces an initial delamination at the interface from which a crack can be propagated during the test.

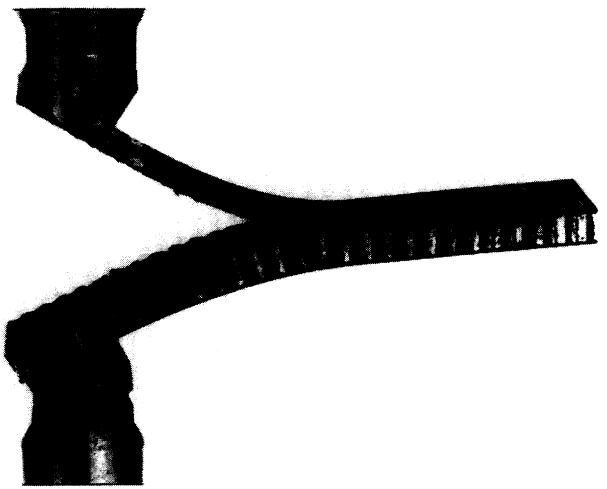

Figure 3. *Double cantilever beam specimen during testing.*

Table 3. Double cantilever beam test matrix.

Test 1	**Test 2**	**Test 3**
NL = 1 ρ_c = 29 kg/m^3 (1.8 pcf) h_c = 0.00635 m (0.25 in.)	NL = 1 ρ_c = 48 kg/m^3 (3.0 pcf) h_c = 0.00953 m (0.375 in.)	NL = 1 ρ_c = 96 kg/m^3 (6.0 pcf) h_c = 0.0127 m (0.5 in.)
Test 4	**Test 5**	**Test 6**
NL = 3 ρ_c = 29 kg/m^3 (1.8 pcf) h_c = 0.00953 m (0.375 in.)	NL = 3 ρ_c = 48 kg/m^3 (3.0 pcf) h_c = 0.0127 m (0.5 in.)	NL = 3 ρ_c = 96 kg/m^3 (6.0 pcf) h_c = 0.00635 m (0.25 in.)
Test 7	**Test 8**	**Test 9**
NL = 5 ρ_c = 29 kg/m^3 (1.8 pcf) h_c = 0.0127 m (0.5 in.)	NL = 5 ρ_c = 48 kg/m^3 (3.0 pcf) h_c = 0.00635 m (0.25 in.)	NL = 5 ρ_c = 96 kg/m^3 (6.0 pcf) h_c = 0.00953 m (0.375 in.)

Specimens of size 25.4×10^{-3} m $\times$ 178×10^{-3} m (1 in. $\times$ 7 in.), were cut from the plates so that the delamination was contained in its first 25.4×10^{-3} m (1 in.) of length. Two groups of tests, each consisting of nine sets of tests, were conducted. In one group the specimens had cracks propagated along their core's *L*-direction, and in the other the crack was propagated in the *W*-direction. In all tests, load was applied at a rate of 0.0127 meters (0.5 inch) per minute cross-head displacement.

A special fixture was manufactured (Figure 3) so that the specimens could be loaded and unloaded with a minimal amount of friction (Avery, 1998). A Greaco-Latin factorial test plan (Schenck, 1961) was used to understand the effects of number of face-sheet plies (NL), the core density (ρ_c), and the core thickness (h_c) on the fracture toughness of the core/face-sheet interface. A 3 x 3 test matrix was constructed such that no two combinations of independent variables were repeated. The three test variables corresponding to each of the 9 tests are shown in Table 3. Five specimens were tested for each test set.

During the test the crack was allowed to propagate, and then the specimen was unloaded. A load-displacement curve, such as the one shown in Figure 4, was generated for each of the specimens. The area under the load-displacement curve, representing work ΔU, was obtained by integration using the trapezoidal method. The crack area created is measured by multiplying the specimen's width by the average crack extension length on each side of the specimen, measured with a pair of dial calipers. The critical strain energy release was computed using the standard equation

$$G_c = \frac{\Delta U}{B\Delta a} \tag{1}$$

where ΔU is the energy used to propagate the crack, B is the specimen's width, and Δa is the crack extension length. The DCB test results are discussed in Section 3. Results for individual tests are available in Avery (1998).

2.4 Flatwise Tensile Test

The specimens for this test were fabricated using 9.525×10^{-3} m (0.375 inch) thick honeycomb material. The combination of core density and number of plies per side alternated between 1.8 and 3.0 pcf, and 1 and 3 plies, respectively, giving 4 possible configurations. A fifth set of specimens was made using the film adhesive between the face-sheet and the core in a single ply face-sheet panel. Thus there were five test sets, each containing 4 specimens. The flatwise tensile tests were conducted at NASA Langley Research Center. The specimens were bonded to a fixture and loaded in tension in the though-the-thickness direction. Displacement was measured using two high-precision LVDT's mounted on each side of the fixture. Loading was continued until complete failure of the composite occurred. The results of flatwise tension tests are discussed in Section 3.2.

2.5 Axial Compression Test

The objective of the axial compression (in-plane compression) tests was to determine the effects of face-sheet delamination on the ultimate load carrying capacity in axial compression. A series of tests were performed on specimens with different core thickness, core density, face-sheet thickness and delamination length. Each specimen was 102×10^{-3} m (4 in.) long and 51×10^{-3} m (2 in.) wide. The goal of these tests was to understand the effects of: (1) face-sheet thickness (t), (2) core

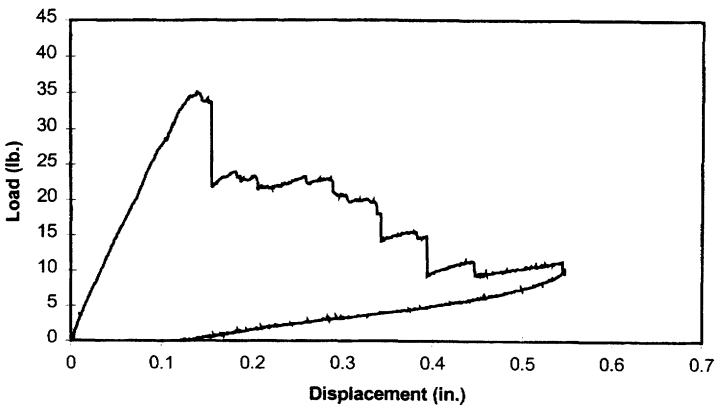

Figure 4. *Typical load-displacement curve of a DCB test.*

Table 4a. Specimen configurations for the axial compression tests.

Test 1		**Test 2**		**Test 3**		**Test 4**	
a_1	t_1	a_2	t_1	a_3	t_1	a_4	t_1
ρ_{c1}	h_{c1}	ρ_{c2}	h_{c2}	ρ_{c3}	h_{c4}	ρ_{c4}	h_{c3}
Test 5		**Test 6**		**Test 7**		**Test 8**	
a_1	t_2	a_2	t_2	a_3	t_2	a_4	t_2
ρ_{c3}	h_{c2}	ρ_{c4}	h_{c1}	ρ_{c1}	h_{c3}	ρ_{c2}	h_{c4}
Test 9		**Test 10**		**Test 11**		**Test 12**	
a_1	t_3	a_2	t_3	a_3	t_3	a_4	t_3
ρ_{c2}	h_{c3}	ρ_{c1}	h_{c4}	ρ_{c4}	h_{c2}	ρ_{c3}	h_{c1}
Test 13		**Test 14**		**Test 15**		**Test 16**	
a_1	t_4	a_2	t_4	a_3	t_4	a_4	t_4
ρ_{c4}	h_{c4}	ρ_{c3}	h_{c3}	ρ_{c2}	h_{c1}	ρ_{c1}	h_{c2}

a: delamination length; t: face-sheet thickness; ρ_c: core density; h_c: core thickness.

thickness (h_c), (3) core density (ρ_c), and (4) delamination length (a) on the compressive strength of the sandwich specimen. To minimize the number of tests to be performed, a Graeco-Latin factorial test plan was used. This test scheme needs 16 test sets for the four variables considered in the problem. From the test results an empirical formula for the compressive strength was derived in terms of the four variables considered in the study. The specimen configurations for each test are presented in Tables 4a and 4b.

A loading fixture was constructed (Avery, 1998) that provided clamped boundary conditions at the ends of the specimen, while allowing the side edges to be free. It also had the benefit of not restricting the visibility of the specimen, allowing for photography of the failing composite. The upper part of the fixture was threaded into the testing machine cross-head, while the lower part of the fixture was threaded directly into the load cell. Bending moments on the load cell caused by

Table 4b. Specimen dimensions and core densities used in the factorial plan.

	a m (in.)	t	ρ_c kg/m^3 (pcf)	h_c m (in.)
1	0.0127 (0.25)	t_p	29 (1.8)	0.00635 (0.25)
2	0.0254 (1.0)	$3t_p$	48 (3.0)	0.009525 (0.375)
3	0.0381 (1.5)	$5t_p$	48 (3.0)	0.009525 (0.375)
4	0.0508 (2.0)	$7t_p$	96 (6.0)	0.0127 (0.5)

t_p = ply thickness = 0.22×10^{-3} m = 8.7×10^{-3} in.

the post-buckling of specimens were corrected for by using an off-axis compensating load cell. The fixture was made entirely from steel to minimize the errors from its compliance.

The specimens were loaded at a rate of 0.3 mm (0.012 in.) per minute cross-head displacement as recommended by the ASTM standard test method C364. Loading was continued until the load dropped to about 75 percent of the maximum achieved load. The results of compression tests are discussed in Section 3.3.

3. RESULTS AND DISCUSSION

3.1 Interfacial Fracture Toughness

The summary of DCB test results are presented in Table 5. These results are the average for five specimens. The results indicate that the interfacial fracture toughness is generally higher for a crack propagated in the *W*-direction than in the *L*-direction. This result may be due to the fact that delamination in the *W*-direction is accompanied by some debonding of the tapes that make up the honeycomb core. Another interesting observation is that the fracture toughness increases with the number of face-sheet plies. This is due to the fact that more resin is available for bonding as the number of face-sheet plies increases.

In order to have a better understanding of the effects of face-sheet plies, core density and core thickness on the interfacial fracture toughness an empirical formula was derived. The Greaco-Latin square test plan allows an empirical function of the following form:

$$G_c = Cf_1(t)f_2(\rho_c)f_3(h_c) \tag{2}$$

where C is a constant and f_1, f_2 and f_3 are functions of corresponding arguments. The three functions are plotted for both *L*- and *W*-directions in Figures 5 through 7.

From Figure 5, it can be seen that the fracture toughness increased significantly from 1 to 3 plies, but as the number of layers increases from 3 to 5, only a slight increase in toughness occurs. This data supports the conclusion also from the through-the-thickness tests discussed in Section 3.2.

Figure 6 reveals interesting results about the influence of core density on the interface fracture toughness. As the core density increases, the fracture toughness decreases. Although a detailed micromechanical analysis may be necessary to explain this phenomenon a qualitative explanation is as follows. The strain energy density is of the form $\sigma^2/2E$, and hence for a given normal stress the energy stored in the core in the vicinity of the crack will be inversely proportional to the Young's modulus of the core. The higher density core material has a higher Young's modulus and hence will store less energy before failure. The fracture toughness is the sum of the surface energy and the energy stored in the core just before the crack

Table 5. Summary of double cantilever beam test results.

Set No.	No. of Layers, NL	Core Thickness, h_c m (in.)	Core Density, ρ_c kg/m^3 (lb/ft^3)	G_c (*L*-dir) N/m (lb/in.)	G_c (*W*-dir) N/m (lb/in.)
1	1	0.00635 (0.25)	29 (1.8)	420 (2.40)	357 (2.04)
2	1	0.009525 (0.375)	48 (3.0)	186 (1.06)	264 (1.51)
3	1	0.0127 (0.5)	96 (6.0)	133 (0.76)	254 (1.45)
4	3	0.009525 (0.375)	29 (1.8)	980 (5.60)	1,139 (6.51)
5	3	0.0127 (0.5)	48 (3.0)	1,050 (6.00)	1,323 (7.56)
6	3	0.00635 (0.25)	96 (6.0)	429 (2.45)	695 (3.97)
7	5	0.0127 (0.5)	29 (1.8)	1,043 (5.96)	1,209 (6.91)
8	5	0.00635 (0.25)	48 (3.0)	963 (5.50)	1,043 (5.96)
9	5	0.009525 (0.375)	96 (6.0)	1,295 (7.40)	929 (5.31)

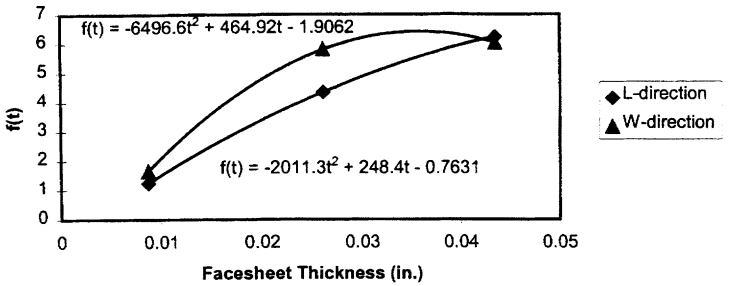

Figure 5. *Critical strain energy release rate function versus face-sheet thickness.*

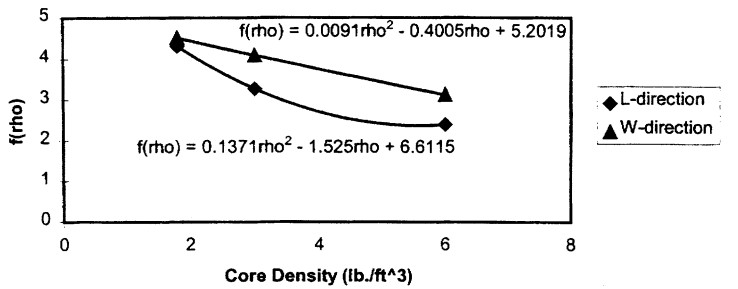

Figure 6. *Critical strain energy release rate function versus core density.*

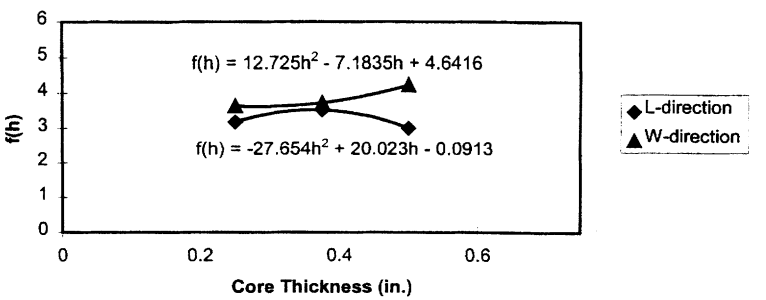

Figure 7. *Critical strain energy release rate function versus core thickness.*

propagation. Thus the high-density core leads to lower fracture toughness of the interface. As one might expect, Figure 7 shows that core thickness has little influence on the fracture toughness of the core/face-sheet interface. Hence the empirical formula in Equation (2) can be modified as

$$G_c = Cf_1(t)f_2(\rho_c) \tag{3}$$

The values of the constant C have been found to be 0.322569 for crack propagation in the L-direction and 0.260664 for the W-direction. The purpose of developing the empirical formula [Equation (3)] is to understand how the number of face-sheet layers, core density and thickness affect the interfacial fracture toughness. This will further help in micromechanical modeling of the fracture behavior of honeycomb core/face-sheet interfaces.

3.2 Flatwise Tensile Tests

The results of flatwise tensile tests are presented in Table 6. The Young's modulus and the tensile strength are actually the effective properties of the core/face-sheet structure. The improvement in the stiffness and tensile strength of the composite with an increase in the number of face-sheet plies should be noticed. The effective Young's modulus seems to increase with the number of face-sheet plies. The increase is 15% for the 1.8 pcf core and about 6% for the 3.0 pcf core. This increase can be explained by the fact that the excess resin and the core form a stiffer composite than the core itself. The effect of adhesive layer on the increase in stiffness is dramatic. In fact there is a 25% increase in stiffness due to the adhesive film. Further, the stiffness is much greater than the three-ply composite also. The increase in stiffness due to increase in core density should not come as a surprise. The effects of number of face-sheet plies on the flatwise tensile strength is also similar to that on stiffness. There is a 10% increase in strength for the 1.8 pcf core

Table 6. Flat-wise tensile test results.

Number of Face-Sheet Plies	Core Density kg/m³ (pcf)	Young's Modulus MPa (ksi)	Tensile Strength MPa (psi)	Percent Debond
1	29 (1.8)	96.8 (14.0)	1.547 (224.4)	68
3	29 (1.8)	111 (16.1)	1.697 (246.1)	1
1	48 (3.0)	196 (28.5)	2.369 (343.5)	90
3	48 (3.0)	207 (30.1)	2.781 (403.3)	21
1+ (film adhesive)	48 (3.0)	246 (35.6)	2.761 (400.4)	0

and 17% increase for the 3 pcf core. The effect of adding the film adhesive to a single ply is the same as that of the 3 ply face-sheet, and in both cases the tensile strength seems to approach that of the core. The strength values can be better understood from the "percentage debond" presented in the last column of Table 6. This is an estimated percentage of the area of the core that failed at the interface. This number is estimated by visually inspecting the face-sheet after failure for remnants of the core. It is a measure of the ratio of the interface strength to the core tensile strength. A higher percentage debond indicates poor interface strength compared to the core, and a lower percentage indicates a stronger interface. For example, one ply with film adhesive produces the strongest interfacial bond. The percentage debond is considerably less for 3 ply specimens compared to the single ply specimens for the same core density. On the other hand the higher the core density the higher the percentage debond.

3.3 Compressive Strength

A summary of the compression test data is presented in Table 7. The table indicates the four test variables, compressive strength and failure mode for each set of tests. The results are averages of six tests for each set. A complete listing of the individual test results can be found in Avery (1998).

Failure of the specimens can be broken down into five major groups or modes. Generally, all the specimens in a set failed in a similar fashion near the same load. The failure modes observed are local antisymmetric buckling (LA), local symmetric buckling (LS), global antisymmetric buckling (GA), global symmetric buckling (GS), and face-sheet failure (FF), where local buckling refers to buckling of the composite near the delamination, and global buckling refers to buckling of the sandwich structure as a whole, generally with the face-sheets parallel with each other. Symmetric buckling refers to a mode shape that is symmetric about a plane perpendicular to the loading axis passing through the mid-span of the specimen. These shapes are illustrated in Figure 8.

The load-deflection diagrams and pictures of buckled specimens for each type of failure mode are presented in Figures 9 through 18. There are four pictures for each specimen labeled a, b, c and d. Loads corresponding to these pictures are marked in the load-deflection diagram also.

Referring to Table 7 it may be noted that specimens 1 through 8 failed locally. These specimens had thin face-sheets, either 1 or 3 plies. Specimen 1 with the shortest delamination (0.5 in.) failed in an antisymmetric mode. All others failed in a symmetric mode. Specimens 9–16 with 3 or 5 ply face-sheets failed in a global mode. When the core thickness was small, an antisymmetric mode was favored. For thick cores the failure was in a symmetric mode. Face-sheet compressive failure occurred in Specimen 13 even before any significant buckling was observed. This specimen had the maximum number of face-sheet plies (7 plies), a thick,

Table 7. Failure loads and failure modes for compression tests.

Test Set	No. of Face-Sheet Plies	Core Thickness m (in.)	Core Density kg/m³ (pcf)	Delam. Length m (in.)	Compressive Strength N/m (lb/in.)	Failure Mode
1	1	0.00635 0.25)	29 (1.8)	0.0127 (0.5)	17,253 (99)	LA
2	1	0.009525 (0.375)	48 (3.0)	0.0254 (1.0)	28,323 (162)	LS
3	1	0.0127 (0.5)	48 (3.0)	0.0381 (1.5)	28,691 (164)	LS
4	1	0.009525 (0.375)	96 (6.0)	0.0508 (2.0)	33,910 (194)	LS
5	3	0.009525 (0.375)	48 (3.0)	0.0127 (0.5)	211,940 (1,210)	LS
6	3	0.00635 (0.25)	96 (6.0)	0.0254 (1.0)	86,983 (497)	LS
7	3	0.009525 (0.375)	29 (1.8)	0.0381 (1.5)	63,232 (361)	LS
8	3	0.0127 (0.5)	48 (3.0)	0.0508 (2.0)	86,983 (439)	LS
9	5	0.009525 (0.375)	48 (3.0)	0.0127 (0.5)	442,796 (2,528)	GS
10	5	0.0127 (0.5)	29 (1.8)	0.0254 (1.0)	212,815 (1,215)	GA
11	5	0.009525 (0.375)	96 (6.0)	0.0381 (1.5)	242,592 (1,385)	GA
12	5	0.00635 (0.25)	48 (3.0)	0.0508 (2.0)	156,345 (893)	GS
13	7	0.0127 (0.5)	96 (6.0)	0.0127 (0.5)	793,109 (4,528)	FF
14	7	0.009525 (0.375)	48 (3.0)	0.0254 (1.0)	406,188 (2,319)	GA
15	7	0.00635 (0.25)	48 (3.0)	0.0381 (1.5)	295,664 (1,688)	GS
16	7	0.009525 (0.375)	29 (1.8)	0.0508 (2.0)	277,273 (1,583)	GA

LA: local, antisymmetric; LS: local, symmetric; GA: global, antisymmetric; GS: global, symmetric; FF: face-sheet failure.

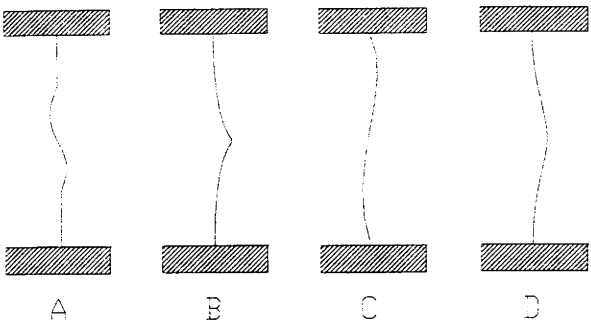

Figure 8. *Different buckling modes. (A) local antisymmetric buckling, (B) local symmetric buckling, (C) global antisymmetric, and (D) global symmetric.*

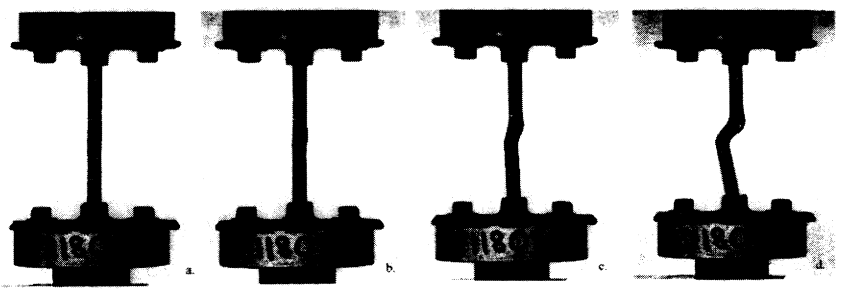

Figure 9. *Compression test, Set 1—local antisymmetric buckling.*

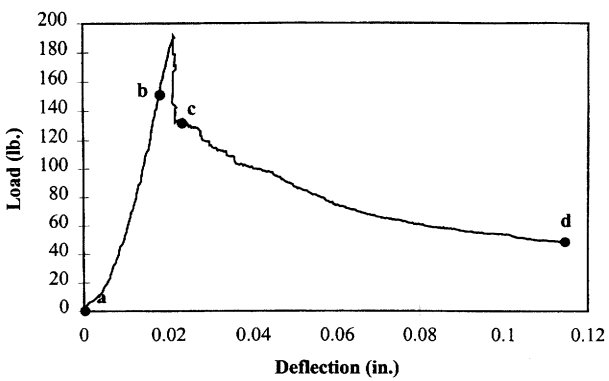

Figure 10. *Load-deflection curve, compression test Set 1.*

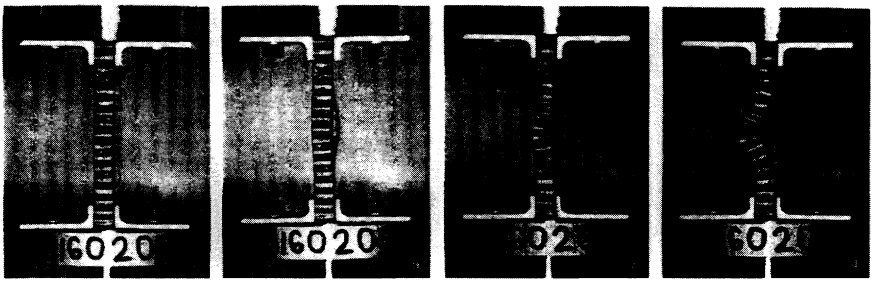

Figure 11. *Compression test, Set 4—local symmetric buckling.*

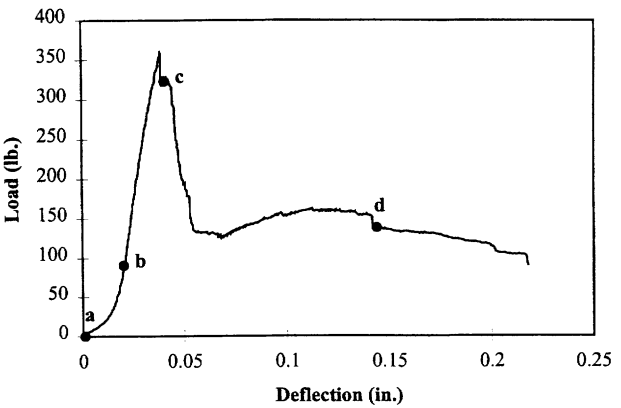

Figure 12. *Load-deflection curve, compression test Set 4.*

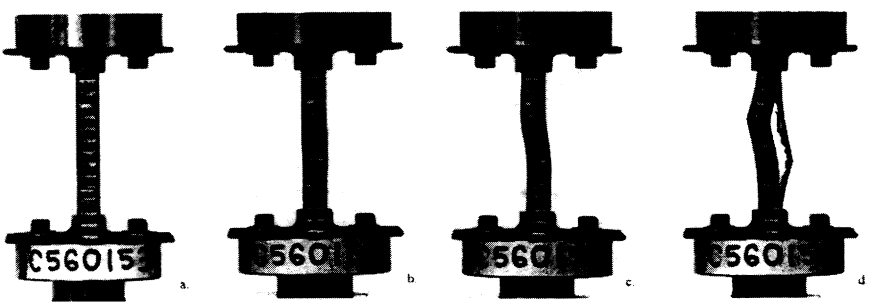

Figure 13. *Compression test, Set 11—global antisymmetric buckling.*

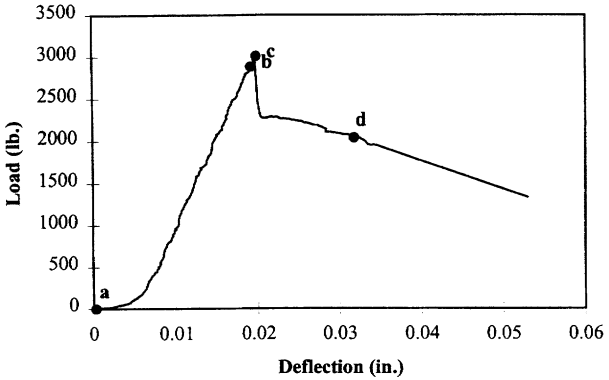

Figure 14. *Load-deflection curve, compression test Set 11.*

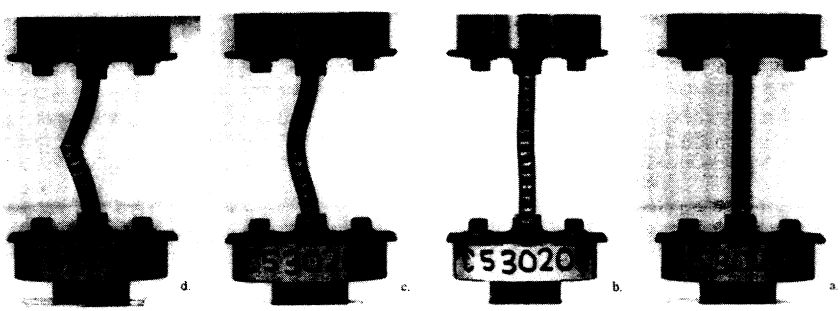

Figure 15. *Compression test, Set 12—global symmetric buckling.*

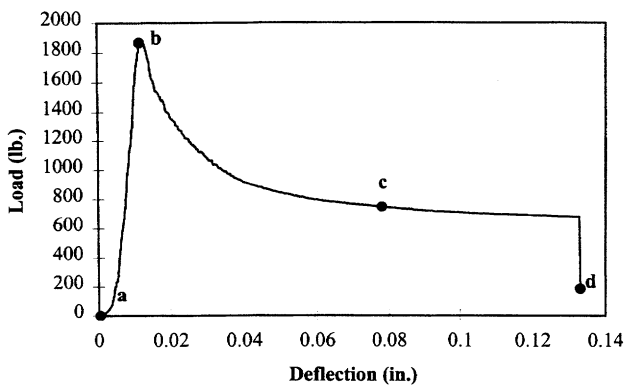

Figure 16. *Load-deflection curve, compression test Set 12.*

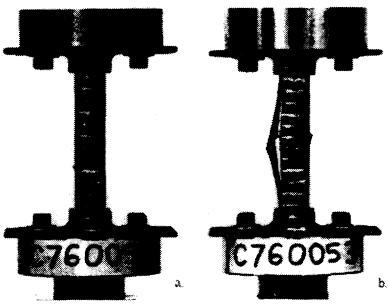

Figure 17. *Compression test, Set 13—face-sheet failure.*

high-density core (0.5 in. thick, 6 pcf) and the shortest delamination (0.5 in.). Thus the global buckling was prevented leading to face-sheet compressive failure. The compressive stress in the ply at the peak load was estimated to be 256 MPa (37 ksi). Since this is much less than the compressive strength of the material (531 MPa or 77 ksi), it is suspected that there should have been some local buckling in the delaminated face-sheet that caused the failure.

Using the results from the Graeco-Latin factorial plan an empirical formula was derived for the ultimate compressive load as a function of the four variables under consideration. The function is of the form:

$$F = Cf_1(t)f_2(a)f_3(\rho_c)f_4(h_c) \tag{4}$$

where C is a constant, and $f_1(t), f_2(a), f_3(\rho_c)$, and $f_4(h_c)$ are functions of corresponding arguments. These functions are plotted in Figures 19 through 22. A polynominal fit for each function is also included in the corresponding figures. The em-

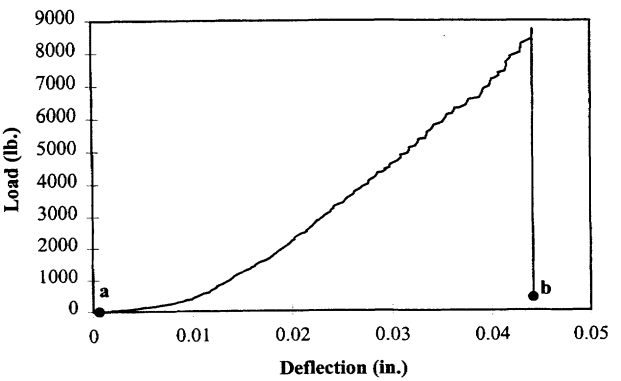

Figure 18. *Load-deflection curve, compression test Set 13.*

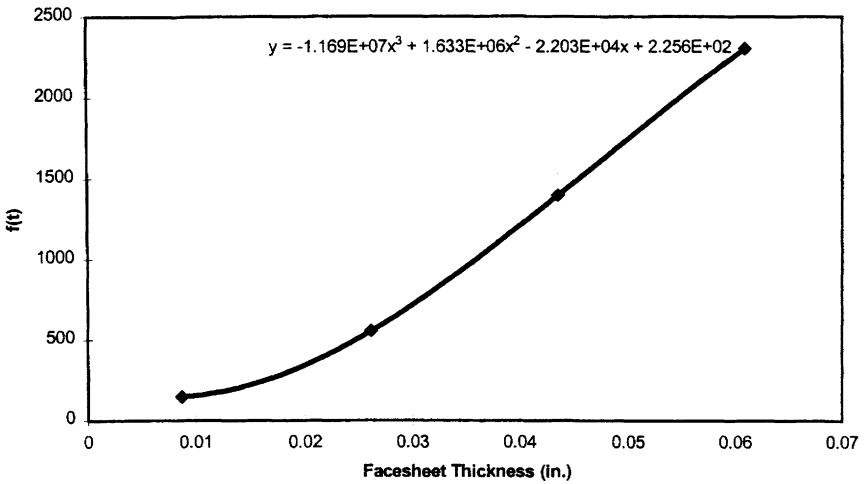

Figure 19. *Effect of face-sheet thickness on ultimate compressive load.*

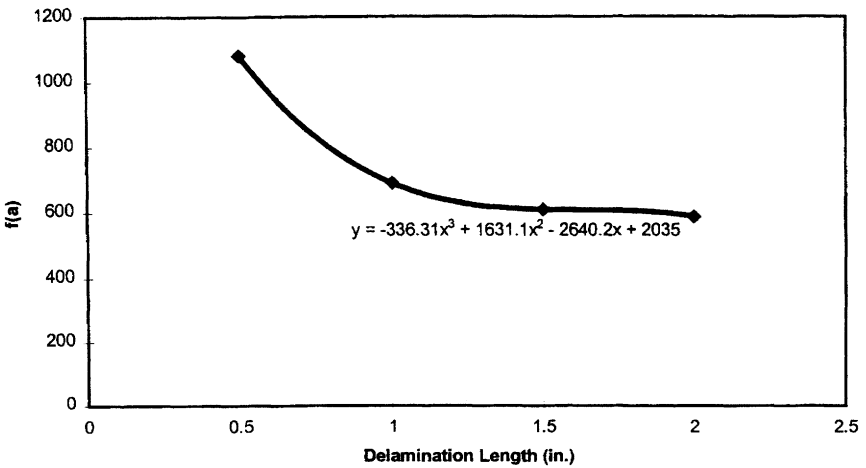

Figure 20. *Effect of delamination length on ultimate compressive load.*

pirical model gives some idea of how each variable affects the ultimate load, and this will be useful in deriving analytical models.

From Figure 19, as we would expect, the failure load is increasing with number of plies or face-sheet thickness. Figure 20 shows the relationship between delamination length and failure load. The delamination length seems to be very critical for short delaminations, however beyond 25.4×10^{-3} m (1 in.), the debond length is less critical to the failure load. The reason is that once the delamination exceeds a certain length, it cannot carry any significant load, and the undelaminated face-sheet and the core becomes critical for the load carrying capacity of the sandwich beam. The next curve, Figure 21, shows the importance of the core density on the load carrying capacity of the composite. There is a definite improvement from the 1.8 pcf core to the 3.0 pcf core, but this dramatic increase slows down in the range of 3 to 6 pcf core density. The effect of core thickness, shown in Figure 22, looks very much like the function for core density previously discussed. An increase in thickness from 0.25 to 0.375 inches dramatically increased the load carrying capacity of the specimen, but when the core thickness was increased beyond that point, the benefit is reduced.

3.4 Analytical Model

A buckling model for delaminated sandwich composite such as the one used in the present study was developed by Hwu and Hu (1992). This model uses a combination of laminate theory and shear deformation theory. One of the limitations of this model is that it assumes symmetry about the beam center, and thus the hori-

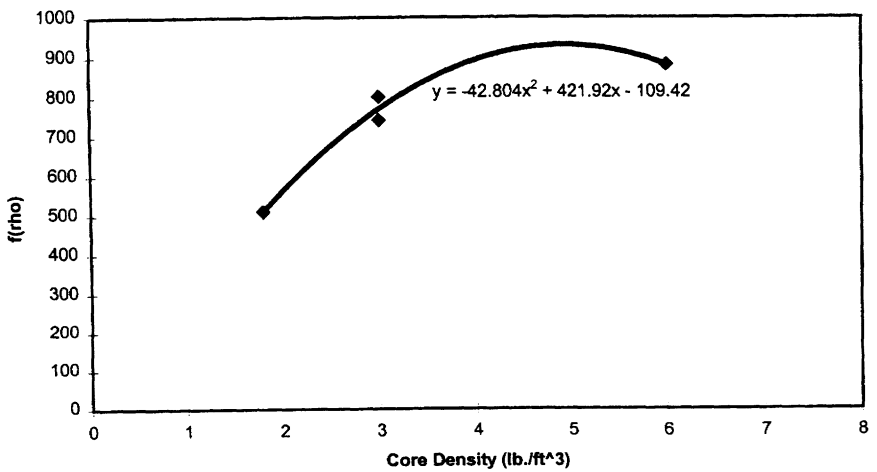

Figure 21. *Effect of core density on ultimate compressive load.*

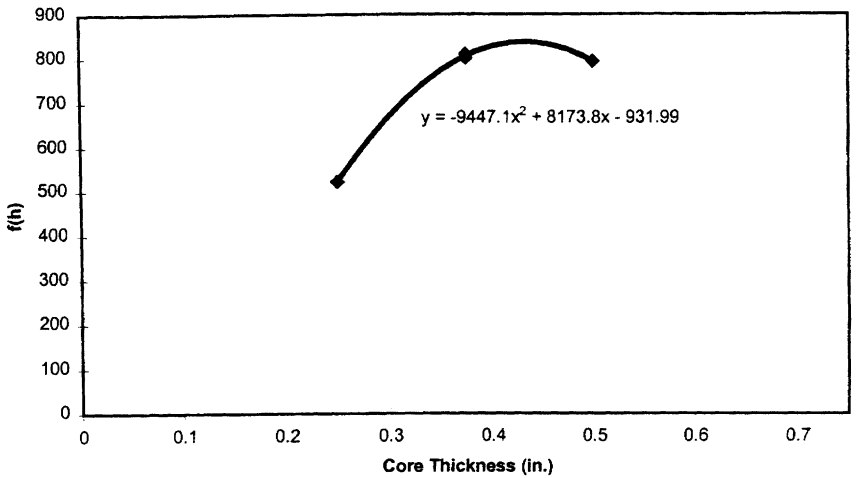

Figure 22. *Effect of core thickness on ultimate compressive load.*

zontal deflections and rotations are set to zero at the center of the beam. The one-half of the beam is divided into three portions as shown in Figure 23. Portion 1 is the intact sandwich beam, 2 is the assemblage of one face-sheet and core, and 3 is the debonded face-sheet. The shear-deformable sandwich beam theory is used for portion 1, and classical lamination theory is used for portions 2 and 3. The core is also assumed to be infinitely stiff in the thickness direction, which is reasonably valid for the aramid honeycomb core material. The reader is referred to Hwu and Hu (1992) for details of derivation of the bucking loads. The buckling loads are given by:

$$P_{cr} = (D_2 + D_3 - D_1)\left[\frac{a}{\lambda_1 \tan \lambda_1 (L-a)} + \frac{ka}{\lambda_2 \tan \lambda_2 a} + \frac{(1-k)a}{\lambda_3 \tan \lambda_3 a}\right]^{-1} \quad (5)$$

where

$$k = \frac{A_3}{A_2 + A_3}, \quad \lambda_1^2 = \frac{P_{cr}}{D_1(1 - P_{cr}/S)}, \quad \lambda_2^2 = \frac{kP_{cr}}{D_2}, \quad \lambda_3^2 = \frac{(1-k)P_{cr}}{D_3}$$

$$A_i = \frac{1}{(A_{11})_i}, \quad B_i = \left(\frac{B_{11}}{A_{11}}\right)_i, \quad D_i = \left(D_{11} - \frac{B_{11}^2}{A_{11}}\right)_i, \quad i = 1,2,3$$

A_{11}, B_{11}, and D_{11} are the extensional stiffness, coupling stiffness and bending stiffness of the laminated composite, and S is the transverse shear stiffness. The sym-

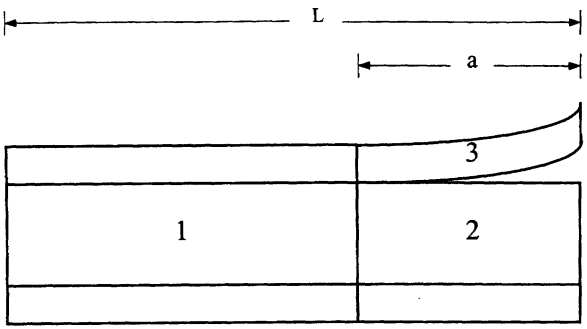

Figure 23. *One-half of the delaminated sandwich beam.*

bol a represents half the crack length and L half the length of the beam. The subscripts i correspond to the three portions of the beam as shown in Figure 23.

Equation (5) was solved using an iterative procedure to obtain the buckling loads, which are presented in Table 8. The "Percentage Difference" in the last column of Table 8 represents the deviation of the experimental results from the lowest

Table 8. Comparison of analytical (symmetric modes) buckling loads to experimental failure loads.

Set	Analytical Buckling Load			Exptl. Failure Load (lb/in.)	% Difference*
	Mode 1 (lb/in.)	Mode 2 (lb/in.)	Mode 3 (lb/in.)		
1	142	568	701	99	43
2	36	143	321	162	-78
3	16	63	143	164	-90
4	9	36	80	194	-95
5	2,465	2,601	2,615	1,210	104
6	956	1,480	3,134	497	92
7	427	655	1,441	361	18
8	240	736	961	439	-45
9	2,552	2,614	2,621	2,528	1
10	1,929	1,947	1,949	1,215	59
11	1,970	2,773	5,098	1,385	42
12	1,103	1,177	1,743	893	24
13	6,752	6,920	6,938	4,528	49
14	2,592	2,620	2,623	2,319	12
15	1,729	1,747	1,749	1,688	2
16	1,456	1,462	1,462	1,583	-8

*Note: the experimental failure loads were compared with the nearest analytical buckling load.

analytical buckling load. In general there is little correlation between the analytical buckling loads and experimental failure loads. Thus the linear buckling load calculated in this way cannot be considered as a conservative estimate of the compressive strength of the sandwich beam. The dimensions of the beam and delamination length used in this study cannot be considered long enough compared to core thickness for the sandwich beam theory to be applicable. At least a two-dimensional plane solid model in conjunction with post-buckling analysis will be required.

4. CONCLUSIONS

Sandwich composites were fabricated using graphite/epoxy as face-sheets and aramid honeycomb as the core material. Debonding between one of the face-sheets and the core were introduced using nonporous Teflon films. The effect of face-sheet thickness and core properties on the interfacial fracture toughness and flatwise tensile strength were studied. The fracture toughness increased with the number of face-sheet plies as the excess resin was available to improve the bonding. On the other hand increase in core density reduced the fracture toughness. The face-sheet thickness did not have any significant effect on the fracture toughness. The interfacial strength also increased with the number of face-sheet plies. When the interface becomes stronger, the failure is shifted to the core, leaving some core material adhering to the face-sheet.

The axial compression tests were performed to determine the load carrying capacity of debonded sandwich beams. When the face-sheets were thin (1 or 3 plies) local buckling is favored. For thick face-sheets (5 or 7 plies) global buckling occurs. When the face-sheet is thick, and also when the core is thick and stiff, face-sheet fails under compression. It was found that the interfacial bonding between the core and the face-sheet was strong enough to prevent disbond growth. The load carrying capacity is limited by the core shear or compressive strength. A simple analytical model based on beam theories was used to predict the buckling loads of the specimens used in the study. The Mode 1 buckling load predicted by the model was close to the experimental failure loads only in specimens in which global buckling occurred. A plane strain finite element post-buckling analysis is underway to predict the behavior of debonded sandwich composites in the entire range of material properties and debond lengths.

ACKNOWLEDGEMENTS

This research was supported by a NASA Langley Research Center Grant (NAG-1-1887) to the University of Florida. The authors are grateful to Mr. Juan R. Cruz, the grant monitor, for his encouragement and many suggestions throughout

the course of the project, and also for his help in performing the flatwise tensile tests.

REFERENCES

Avery, J. L., 1998. "Compressive Failure of Delaminated Sandwich Composites," Master of Science thesis, Department of Aerospace Engineering, Mechanics & Engineering Science, University of Florida, Gainesville, Florida.

Chen, H. P., 1993. "Transverse Shear Effects on Buckling and Postbuckling of Laminated and Delaminated Plates," *AIAA Journal,* 31(1):163–169.

Hwu, C. and J. S. Hu. 1992. "Buckling and Postbuckling of Delaminated Composite Sandwich Beams," *AIAA Journal,* 30(7):1901–1909.

Kardomateas, G. A. 1990. "Postbuckling Characteristics in Delaminated Kevlar/Epoxy Laminates: An Experimental Study," *J. Composites Technology & Research,* 12(2):85–90.

Kassapoglou, C., 1988. "Buckling, Post-Buckling and Failure of Elliptical Delaminations in Laminates under Compression," *Composite Structures,* 19:139–159.

Kim, W. C. and C. K. H. Dharan, 1992. " Facesheet Debonding Criteria for Composite Sandwich Panels under In-Plane Compression," *Engineering Fracture Mechanics,* 42(4):642–652.

Minguet, P., J. Dugundji and P. A. Lagace. 1987. "Buckling and Failure of Sandwich Plates with Graphite-Epoxy Faces and Various Cores," *J. Aircraft,* 25(4):372–379.

Schenck, H., 1961. *Theories of Engineering Experimentation,* McGraw-Hill, New York.

Simitses, G. J., S. Sallam and W. L. Yin, 1985. "Effect of Delamination of Axially Loaded Homogeneous Laminated Plates," *AIAA Journal,* 23(9):1437–1444.

Sleight, D. W. and J. T. Wang, 1995. "Buckling Analysis of Debonded Sandwich Panel under Compression," *NASA Technical Memorandum 4701.*

Yin, W.-L., S. N. Sallam and G. J. Simitses, 1986. "Ultimate Axial Load Capacity of a Delaminated Beam-Plate," *AIAA Journal,* 24(1):123–128.